J. Fluid Mech. (2002), *vol.* 462, *pp.* 245–254.
DOI: 10.1017/S0022112002008911 Printed in the United Kingdom

Area–volume properties of fluid interfaces in turbulence: scale-local self-similarity and cumulative scale dependence

By HARIS J. CATRAKIS, ROBERTO C. AGUIRRE AND JESUS RUIZ-PLANCARTE

Aeronautics and Fluid Dynamics Laboratories, University of California, Irvine, CA 92697, USA

(Received 1 March 2002 and in revised form 7 April 2002)

Area–volume properties of fluid interfaces are investigated to quantify the scale-local and cumulative structure. An area–volume density $g_3(\lambda)$ and ratio $\Omega_3(\lambda)$ are introduced to examine the interfacial behaviour as a function of scale λ or across a range of scales, respectively. These measures are demonstrated on mixed-fluid interfaces from whole-field $\sim 1000^3$ three-dimensional space–time concentration measurements in turbulent jets above the mixing transition, at $Re \sim 20\,000$ and $Sc \sim 2000$, recorded by laser-induced-fluorescence and digital-imaging techniques, with Taylor's hypothesis applied. The cumulative structure is scale dependent in $\Omega_3(\lambda)$, with a dimension $D_3(\lambda)$ that increases with increasing scale. In contrast, the scale-local structure exhibits self-similarity in $g_3(\lambda)$ with an exponent $\alpha_g \approx 1.3$ for these interfaces. The scale dependence in the cumulative structure arises from the large scales, while the self-similarity corresponds to the small-scale area–volume contributions. The small scales exhibit the largest area–volume density and provide the dominant contributions to the total area–volume ratio, which corresponds to ~ 10 times the area of a purely large-scale interface for the present flow conditions. The self-similarity in the scale-local structure at small scales provides the key ingredient to extrapolate the area–volume behaviour to higher Reynolds numbers.

1. Introduction

Fluid interfaces generated by turbulent flows are known to exhibit complex dynamics and structure over a wide range of scales (e.g. Sreenivasan 1991; Vassilicos & Hunt 1991; Yoda, Hesselink & Mungal 1994; Dalziel, Linden & Youngs 1999; Villermaux & Innocenti 1999; Catrakis & Bond 2000). The behaviour of the interfaces and their relation to the flow dynamics provide a physical point of view useful in studies of turbulence. One of the principal challenges in turbulence is to bridge the gap between the knowledge of the flow dynamics that is beginning to be acquired at moderate Reynolds numbers and what needs to be known at large values of the Reynolds number. Such questions have usually been addressed in terms of correlation tensors, structure functions, and spectra (e.g. Frisch 1995; Sreenivasan & Antonia 1997; and references therein). Physically, and from the point of view of practical applications, a crucial feature is the structure of the turbulent fluid interfaces. How convoluted are they in turbulent flows? What are the relative contributions of the large-scale and small-scale flow dynamics to the interfacial structure? How does one extrapolate knowledge of the interfacial behaviour to higher Reynolds numbers?

Turbulent fluid interfaces are of interest both fundamentally and practically (e.g. Pope 1988; Roshko 1991; Sreenivasan 1991; Dimotakis 2000). The term fluid interfaces covers any isosurfaces or regions in the flow associated with a given fluid or flow property, such as concentration, density, velocity or vorticity interfaces. For example, mixed-fluid interfaces correspond to isoconcentration surfaces in turbulent mixing. Knowledge of the behaviour of mixed-fluid interfaces is needed for physically based descriptions and predictions of mixing in turbulence. Useful interfacial properties include geometrical statistics such as the area–volume ratio, fractal or scale-dependent coverage dimensions, and distributions of interfacial scales (e.g. Mandelbrot 1975; Takayasu 1982; Pope 1988; Sreenivasan, Ramshankar & Meneveau 1989; Sreenivasan 1991; Vassilicos & Hunt 1991; Catrakis & Dimotakis 1996, 1998; Villermaux & Innocenti 1999; Catrakis 2000). Such properties quantify the interfacial behaviour and are important in various applications such as aero-optics (e.g. Dimotakis, Catrakis & Fourguette 2001; Jumper & Fitzgerald 2001), mixing (e.g. Villermaux & Innocenti 1999), and flow control (e.g. Gad el Hak 2000).

The large-scale as well as small-scale interfacial properties are significant in practice. The interfacial large-scale structure is important for transport and entrainment (e.g. Brown & Roshko 1974), while the small-scale behaviour can influence the total interfacial area (e.g. Catrakis & Dimotakis 1998). The behaviour across the entire range of interfacial scales determines the mixing efficiency, or fraction of mixed fluid, in the flow. A basic issue concerning small-scale interfacial behaviour is the extent to which the interfaces exhibit scale independence, i.e. self-similarity, or scale dependence. The original proposals of interfacial self-similarity can be traced to Richardson (1922), Welander (1955), and Mandelbrot (1975). This continues to be an active subject of study with a number of reports indicating self-similar behaviour (e.g. Sreenivasan & Meneveau 1986; Vassilicos & Hunt 1991; Frederiksen, Dahm & Dowling 1996, 1997; Dalziel *et al.* 1999) while other studies suggest scale-dependent behaviour (e.g. Takayasu 1982; Miller & Dimotakis 1991; Catrakis & Dimotakis 1996). Scale independence of the interfaces would enable the use of power-law descriptions in terms of constant fractal dimensions (e.g. Sreenivasan 1991), while scale-dependent behaviour would require knowledge of the distribution of interfacial scales (e.g. Catrakis 2000). These approaches would permit extrapolation of the interfacial properties to higher Reynolds numbers.

In the present work, area–volume properties of fluid interfaces are considered with emphasis on the scale-local as well as cumulative structure in order to investigate self-similarity and the relative contributions of the large-scale and small-scale interfacial features to the area–volume behaviour. In § 2, scale-local and cumulative measures are introduced to identify interfacial area–volume contributions as a function of scale or across a range of scales, respectively. In § 3, these area–volume measures are demonstrated on mixed-fluid interfaces derived from whole-field $\sim 1000^3$ three-dimensional space–time concentration measurements in turbulent jets above the mixing transition at $Re \sim 20\,000$ and $Sc \sim 2000$, with Taylor's hypothesis applied. Results are presented on both the scale-local and cumulative interfacial structure and area–volume properties. Some general implications are discussed in the conclusions.

2. Proposed area–volume measures of fluid interfaces

Quantitative examinations of self-similarity of fluid interfaces in turbulent flows have relied mostly on box-counting statistics (e.g. Sreenivasan 1991; Vassilicos & Hunt 1991; Dalziel *et al.* 1999; Villermaux & Innocenti 1999; Catrakis & Bond 2000), in

particular the dimension $D_d(\lambda)$ derived from the coverage $N_d(\lambda)$, where d denotes the Euclidean dimension of the interfaces, e.g. $d = 3$. A large-scale bounding box of size δ_b, containing the interface, is partitioned into λ-scale boxes and $N_3(\lambda)$ is the number of λ-scale boxes necessary to cover the interface, with $N_3(\delta_b) = 1$. Normalized by the total number of partition boxes at scale λ, $N_3(\lambda)$ yields the interfacial coverage fraction $F_3(\lambda) \equiv N_3(\lambda)\,(\lambda/\delta_b)^3$. It is the probability that a λ-box contains part of the interface. The coverage dimension $D_3(\lambda)$ is a logarithmic scale derivative of $N_3(\lambda)$, i.e.

$$D_3(\lambda) \equiv -\frac{\mathrm{d}\log N_3(\lambda)}{\mathrm{d}\log\lambda} \equiv 3 - \frac{\mathrm{d}\log F_3(\lambda)}{\mathrm{d}\log\lambda} \tag{2.1}$$

(e.g. Takayasu 1982). This quantity is often employed to examine self-similarity and is regarded as the effective dimensionality of the interface as a function of scale. It may be called a generalized fractal dimension in the sense that it need not be scale independent. For mixed-fluid interfaces, it satisfies the bounds $2 \leqslant D_3(\lambda) \leqslant 3$, where 2 is the topological dimension of the interfaces in three dimensions. If a range of scales is found where $D_3(\lambda)$ is a constant, i.e. if $N_3(\lambda) \sim \lambda^{-D_3}$, then D_3 can be identified as the fractal dimension associated with self-similar structure of the interfaces at those scales. In the general case, the behaviour of $D_3(\lambda)$ may be related to a distribution of interfacial scales in the sense of level-crossing spacings (e.g. Catrakis 2000).

To quantify the interfacial area–volume behaviour, we propose a dimensionless area–volume ratio $\Omega_3(\lambda)$ defined as a function of scale λ, in terms of a box-counting measure of the interfacial area, $A_3(\lambda) \equiv \lambda^2 N_3(\lambda)$, normalized by the bounding-box volume, $V_b \equiv \delta_b^3$:

$$\Omega_3(\lambda) \equiv \frac{A(\lambda)}{V_b^{2/3}} = \left(\frac{\lambda}{\delta_b}\right)^2 N_3(\lambda), \quad \text{with} \quad \alpha_\Omega(\lambda) \equiv -\frac{\mathrm{d}\log\Omega_3(\lambda)}{\mathrm{d}\log\lambda} = D_3(\lambda) - 2, \tag{2.2}$$

where $0 \leqslant \alpha_\Omega(\lambda) \leqslant 1$ is the logarithmic derivative associated with the area–volume ratio $\Omega_3(\lambda)$. This is a generalization of the total shape complexity, or total area–volume ratio, employed by Catrakis & Dimotakis (1998). The bounds of the proposed area–volume ratio will be $1 = \Omega_3(\delta_b) \leqslant \Omega_3(\lambda) \leqslant \Omega_3(0) \equiv \Omega_{3,\mathrm{tot}}$ where $\Omega_{3,\mathrm{tot}}$ denotes the total value corresponding to the interfacial area across the entire range of scales. The area–volume ratio $\Omega_3(\lambda)$ increases with decreasing scale because $\Omega_3(\lambda)$, as well as $N_3(\lambda)$, measure the cumulative interfacial structure. The value of $\Omega_3(\lambda)$ at a given scale is influenced by all interfacial features above that scale, because $N_3(\lambda)$ is sensitive to the interfacial features above the scale λ. Both $N_3(\lambda)$ and $\Omega_3(\lambda)$, therefore, contain interfacial information from scales larger than or equal to λ, in particular including the large scales of the flow.

Is there a way to quantify the scale-local, as opposed to cumulative, area–volume behaviour? To answer this, we introduce an area–volume density $g_3(\lambda)$ as the scale-local contribution from interfacial features in the differential scale range $\{\lambda, \lambda + \mathrm{d}\lambda\}$ to the area–volume ratio. This scale-local quantity is obtained from the cumulative area–volume ratios at scales λ and $\lambda + \mathrm{d}\lambda$ as $\Omega_3(\lambda) \equiv \Omega_3(\lambda + \mathrm{d}\lambda) + g_3(\lambda)\mathrm{d}\lambda$, i.e.

$$g_3(\lambda) \equiv -\frac{\mathrm{d}\Omega_3(\lambda)}{\mathrm{d}\lambda}, \quad \text{with} \quad \alpha_g(\lambda) \equiv -\frac{\mathrm{d}\log g_3(\lambda)}{\mathrm{d}\log\lambda}, \tag{2.3}$$

where $\alpha_g(\lambda)$ is a logarithmic derivative of $g_3(\lambda)$, cf. (2.2). If $\alpha_g(\lambda) = \text{const.}$, then α_g can be interpreted as the area–volume density exponent with $g_3(\lambda) \sim \lambda^{-\alpha_g}$. More generally, $g_3(\lambda) = \exp\{\int_\lambda^{\delta_b} \alpha_g(\lambda')\mathrm{d}\lambda'/\lambda'\}/\delta_b$, valid even if α_g is scale dependent. Whereas $\Omega_3(\lambda)$

characterizes the cumulative area–volume contributions, $g_3(\lambda)$ provides the means to quantify the scale-local interfacial contributions to the area–volume ratio.

At the large scales, the area–volume ratio behaves as $\Omega_3(\lambda \to \delta_b) \sim (\lambda/\delta_b)^{-1} \to 1$, since $N_3(\lambda \to \delta_b) \sim (\lambda/\delta_b)^{-3} \to 1$, while at the smallest scales $\Omega_3(\lambda \to 0) \to \Omega_{3,\mathrm{tot}} =$ const. The corresponding interfacial area–volume density contributions are $g_3(\lambda \to \delta_b) = 1/\delta_b$ and $g_3(\lambda \to 0) = 0$, resulting in $-\infty \leqslant \alpha_g(\lambda) \leqslant 2$. The α_g limits are different from the α_Ω bounds, cf. (2.2); in particular α_g can be negative. At scales where $\alpha_g \geqslant 1$, $\alpha_g(\lambda)$ can be interpreted as a scale-local dimension. Specifically, if the interfacial coverage is $N_3(\lambda) \sim \lambda^{-D_3}$, with $D_3 =$ const., then $D_3 = \alpha_g + 1$. In general, however, the interfacial coverage dimension $D_3(\lambda)$ will not necessarily be equivalent to the area–volume density exponent $\alpha_g(\lambda)$, i.e. $D_3(\lambda) \neq \alpha_g(\lambda)+1$. This is because $\Omega_3(\lambda)$ and $N_3(\lambda)$ are cumulative quantities coupling interfacial information across different scales, whereas $g_3(\lambda)$ and $\alpha_g(\lambda)$ are scale-local measures. In fact, inverting (2.3) and using (2.2),

$$\Omega_3(\lambda) = 1 + \int_\lambda^{\delta_b} g_3(\lambda')\mathrm{d}\lambda', \quad \text{and} \quad D_3(\lambda) = 2 + \frac{\lambda g_3(\lambda)}{1 + \int_\lambda^{\delta_b} g_3(\lambda')\mathrm{d}\lambda'}, \tag{2.4}$$

showing explicitly that $\Omega_3(\lambda)$ as well as the dimension $D_3(\lambda)$ are scale cumulative. In particular, these cumulative quantities are affected by contributions from the large scales. In contrast, $g_3(\lambda)$ can be used to separate the small-scale properties from the large-scale behaviour. The area–volume density $g_3(\lambda)$ and exponent $\alpha_g(\lambda)$ enable the scale-local examination of the interfacial area–volume contributions and can be expected to be particularly useful for determining the presence of self-similarity.

3. Application to measurements of mixed-fluid interfaces

The proposed area–volume quantities can be applied to various fluid interfaces in turbulence. We demonstrate them here on mixed-fluid interfaces derived from whole-field high-resolution three-dimensional space–time concentration measurements in turbulent jets above the mixing transition. The flow facility, experiments, and imaging technique are described in detail in Catrakis *et al.* (2002), and are briefly summarized here for completeness. The facility consists of a 6 ft diameter, 9 ft high octagonal tank with extensive optical access and was operated in a blow-down manner to generate a turbulent water jet with exit velocity $U_0 = 8\,\mathrm{m\,s^{-1}}$ from a contoured nozzle of exit diameter $d = 2.54\,\mathrm{mm}$, resulting in a Reynolds number $Re \sim 20\,000$ which is above the mixing transition (e.g. Roshko 1991; Dimotakis 2000). The imaging technique relied on laser-induced fluorescence of disodium fluorescein with a Schmidt number $Sc \sim 2000$ (e.g. Sreenivasan & Meneveau 1986; Catrakis & Dimotakis 1996). Three-dimensional space–time x, y, t imaging was conducted in the far field ($z/d \sim 500$) by illuminating the x, y similarity plane of the jet, i.e. normal to the jet axis, with a laser sheet and recording the concentration field in this plane continuously in time with a 1008×1018-pixel, 10-bit CCD sensor (Kodak KAI-1010M) operating at 30 frames/s for a total of 972 images per run. Each $\sim 1000^3$ whole-field data set was calibrated, normalized, and processed to extract outer mixed-fluid interfaces as isoconcentration surfaces marking the boundary between mixed fluid and pure ambient fluid. In order to apply Taylor's hypothesis in time, the imaging rate was chosen to match the mean velocity of the outer interfaces.

Figure 1 shows an example of a two-dimensional spatial x, y concentration field extracted from the whole-field $\sim 1000^3$ three-dimensional space–time measurements.

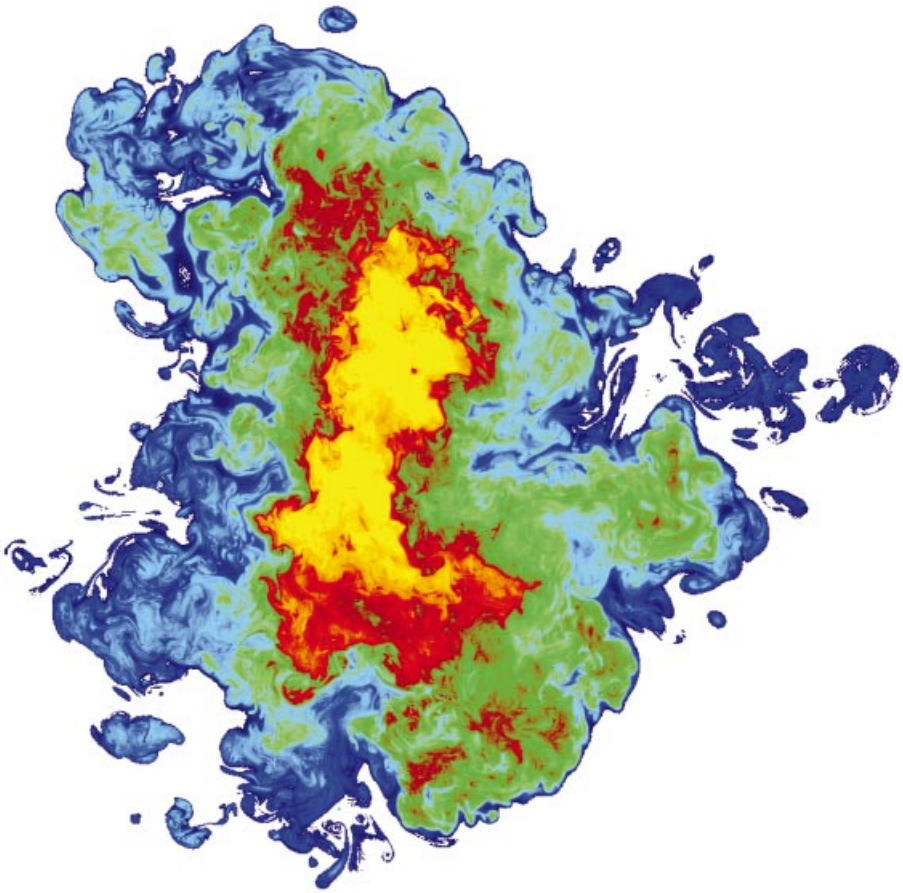

FIGURE 1. A two-dimensional spatial x, y concentration-field image extracted from whole-field $\sim 1000^3$ three-dimensional space–time x, y, t measurements in the similarity plane of a turbulent jet at $Re \sim 20\,000$ and $Sc \sim 2000$, at a far-field downstream distance of $z/d \sim 500$ where d is the jet nozzle diameter. The transverse extent of the jet in the image is ~ 0.5 m. The colours from blue to yellow denote increasing levels of jet-fluid concentration, and were applied to aid the eye in visualizing the concentration field as well as the mixed-fluid interfaces. White denotes pure ambient fluid. The outer interface, between mixed fluid and pure fluid, is visible as the convoluted boundary between blue and white.

The outer interface is visible as the convoluted boundary between mixed fluid and pure ambient fluid, i.e. the interface between blue and white in figure 1. Such two-dimensional interfaces have been studied before, e.g. Sreenivasan & Meneveau (1986) and Catrakis & Dimotakis (1996). An example of the evolution in time of the outer interface is shown in figure 2 which depicts the whole-field dynamics of the interface, with time normal to the page, and corresponds to the passage of about three large-scale structures through the interior of the outer interface. Large-scale as well as small-scale area–volume features of the outer interfaces are evident in figure 3 which is a whole-field opaque rendering of a three-dimensional space–time x, y, t outer interface. The present data enable an examination of the large-scale and small-scale contributions to the area–volume behaviour.

The area–volume measures of § 2 were applied to the outer mixed-fluid interfaces. Box-counting was performed in three dimensions, using Taylor's hypothesis in time,

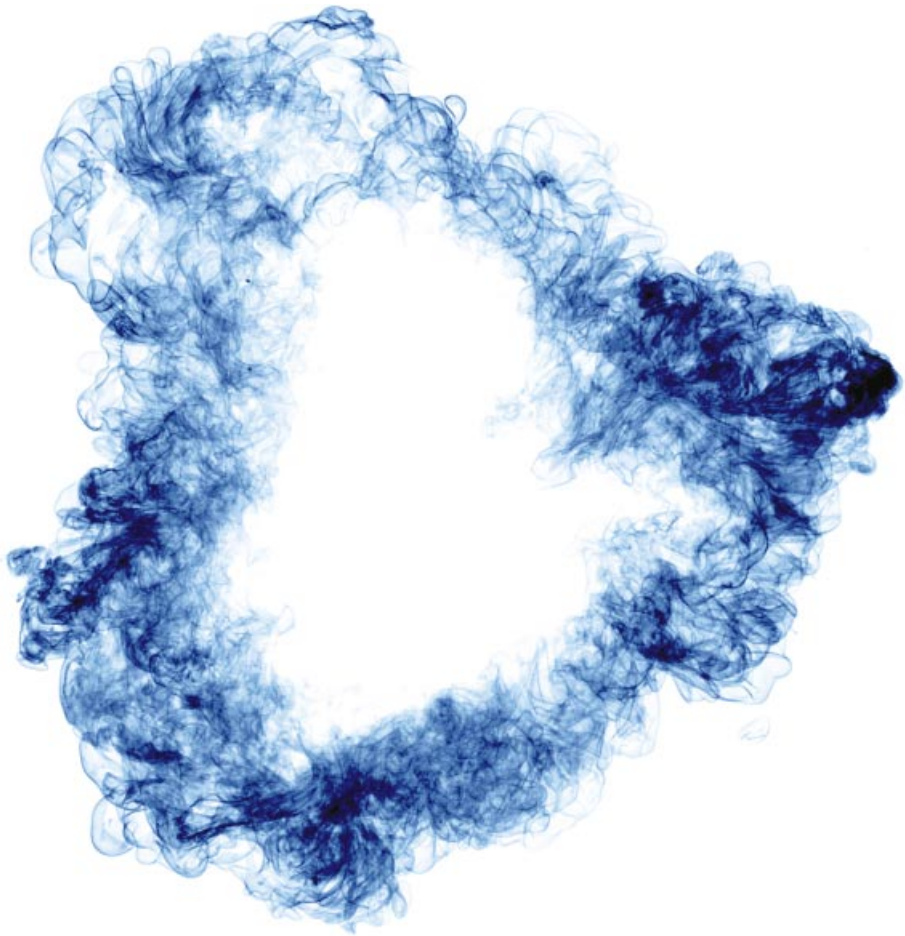

FIGURE 2. A transparent visualization showing the evolution in time of the outer interface at $Re \sim 20\,000$ and $Sc \sim 2000$, extracted from a data set of $\sim 1000^3$ three-dimensional space–time x, y, t concentration measurements. The visualization spans the entire jet diameter and the dynamics correspond to the passage of about three large-scale structures through the higher-speed interior of the outer interface. The view shown is along the time axis and the blue colour corresponds to the outer-interface fluid, cf. figure 1.

to evaluate all the quantities discussed in § 2, i.e. the coverage $N_3(\lambda)$, the coverage fraction $F_3(\lambda)$, the cumulative area–volume ratio $\Omega_3(\lambda)$ with exponent $\alpha_\Omega(\lambda)$, and the scale-local area–volume density $g_3(\lambda)$ with exponent $\alpha_g(\lambda)$. Anisotropic box-counting measures (e.g. Catrakis 2000) were not examined since the focus of this study was on scale-independence/-dependence. In general, there will be a distribution of directions at each scale and the results below correspond to properties averaged over the direction distribution. Ensemble-averaged results for the box counts and area–volume measures are presented in figure 4. Interfacial scales are normalized by the ensemble-averaged bounding-box scale δ_b. From the coverage $N_3(\lambda)$ and coverage fraction $F_3(\lambda)$, in figures 4(a) and 4(b), the area–volume measures were derived. The area–volume ratio $\Omega_3(\lambda)$ in figure 4(c) exhibits scale dependence, as is also evident in figure 4(d) which shows that $\alpha_\Omega(\lambda)$ increases continuously with increasing scale and, therefore, $D_3(\lambda) \equiv \alpha_\Omega(\lambda) + 2$ is also scale dependent; the uncertainty in $\alpha_\Omega(\lambda)$ is

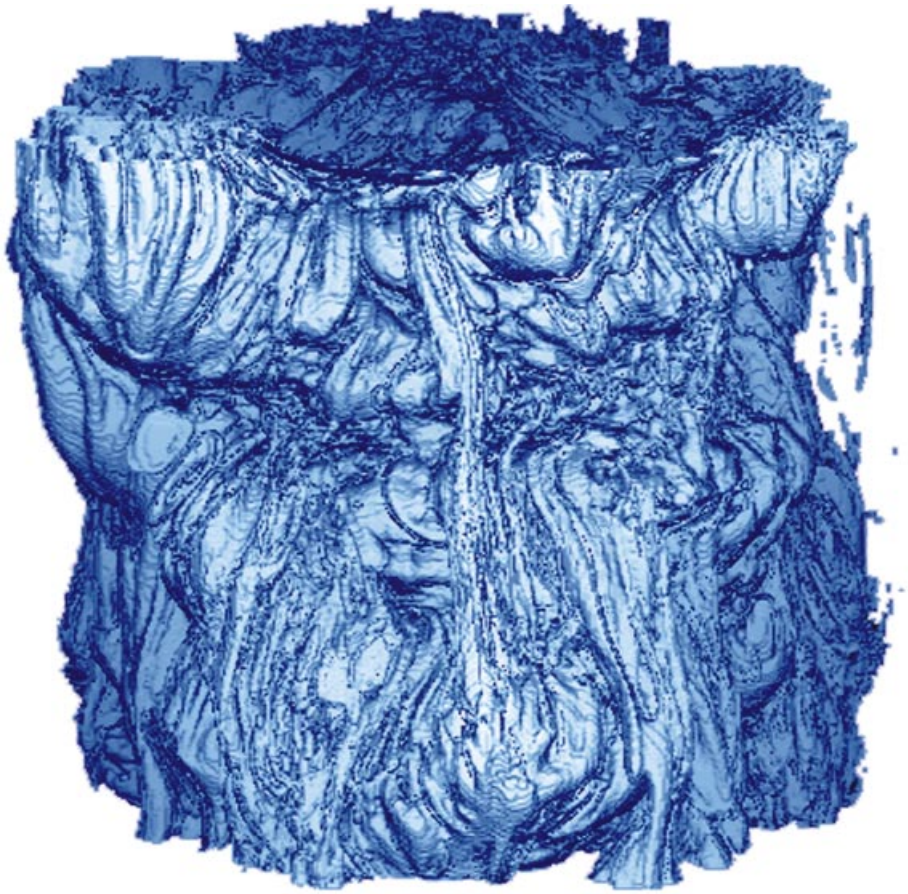

FIGURE 3. Large-scale as well as small-scale area–volume features of the outer interface are evident in this visualization. The image shown is a whole-field opaque rendering derived from the $\sim 1000^3$ space–time x, y, t concentration measurements and the view of the outer interface shown is normal to the time axis, cf. figure 2. Early times are at the bottom. The corresponding streamwise direction is from top to bottom.

estimated at ± 0.02. The cumulative behaviour is, therefore, scale dependent. In contrast, the scale-local area–volume density $g_3(\lambda)$, shown in figure 4(e), exhibits power-law scaling as indicated by the near-constant value $\alpha_g(\lambda) \approx 1.3$ in figure 4(f); note that $\alpha_g(\lambda) < 1$ at the smallest scales as expected from the analysis in §2. The scale-local area–volume contributions, therefore, exhibit self-similarity. If $D_3(\lambda)$ were constant, then $\alpha_g \approx 1.3$ would correspond to $D_3 = \alpha_g + 1 \approx 2.3$. This dimension value is in very close agreement with previous results (e.g. Sreenivasan & Meneveau 1986; Prasad & Sreenivasan 1990). For a scale-dependent $D_3(\lambda)$, as is the case here, $D_3(\lambda)$ is not equivalent to $\alpha_g(\lambda)$. As discussed in § 2, $D_3(\lambda) \neq \alpha_g(\lambda) + 1$ in general because $D_3(\lambda)$ couples interfacial features across different scales. Yet, the results in figures 4(d) and 4(f) demonstrate that scale-local self-similarity is consistent with cumulative scale dependence in the area–volume behaviour. The often-employed coverage dimension $D_3(\lambda)$ is in this case not sufficient to detect the self-similarity in the interfacial structure. The area–volume density $g_3(\lambda)$ and exponent $\alpha_g(\lambda)$ enable a separation of the small-scale structure from the large-scale behaviour and suggest that the cumulative scale dependence arises from the large

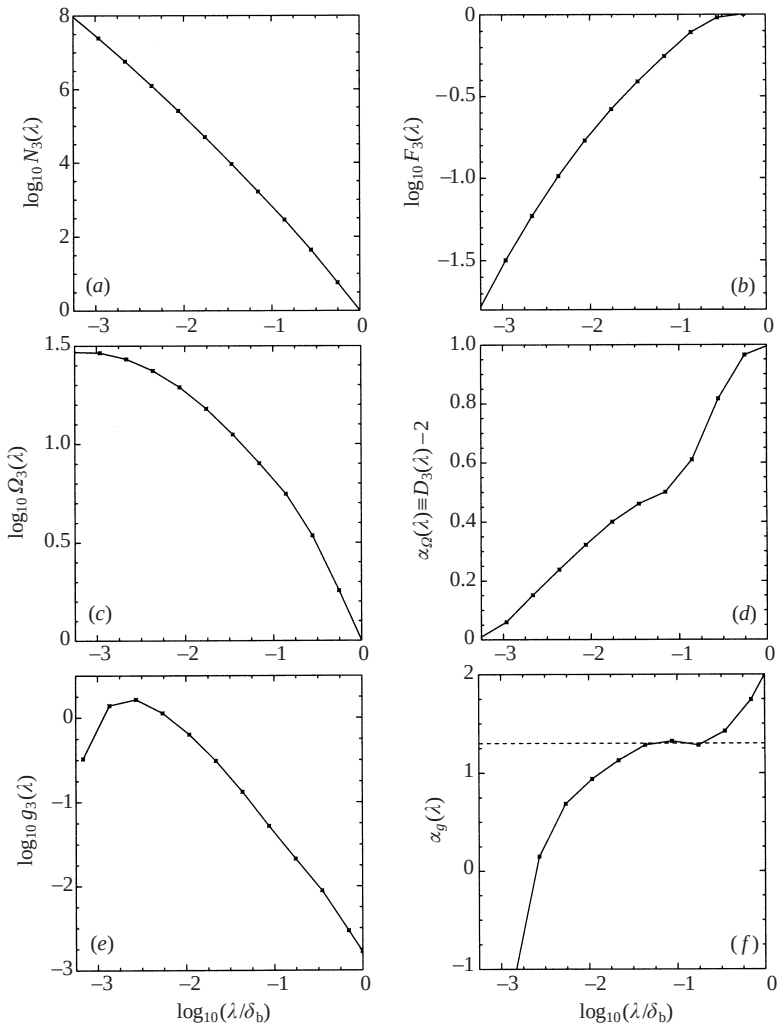

FIGURE 4. Ensemble-averaged statistics of mixed-fluid interfaces: (*a*) coverage $N_3(\lambda)$; (*b*) coverage fraction $F_3(\lambda)$; (*c*) cumulative area–volume ratio $\Omega_3(\lambda)$; (*d*) area–volume exponent $\alpha_\Omega(\lambda) \equiv D_3(\lambda)-2$, where $D_3(\lambda)$ is the coverage dimension; (*e*) scale-local area–volume density $g_3(\lambda)$; (*f*) scale-local area–volume density exponent $\alpha_g(\lambda)$, with the dashed line at $\alpha_g = 1.3$.

scales while the self-similarity corresponds to the small scales, cf. (2.4) and figures 4(*d*) and 4(*f*).

The largest area–volume density is associated with the small scales which provide the dominant contributions to the total area–volume ratio, cf. figure 4(*e*). For the present interfaces, this is $\log_{10}\Omega_{3,\mathrm{tot}} \approx 1.47$ or $\Omega_{3,\mathrm{tot}} \approx 30$, cf. figure 4(*c*). This corresponds to $(\Omega_{3,\mathrm{tot}}\,\delta_b^2)/(\pi\delta_b^2) \sim 10$ times the area of a purely large-scale interface, cf. (2.2), consistent with two-dimensional measurements (e.g. Paizis & Schwarz 1974; Catrakis & Dimotakis 1996). This order-of-magnitude increase in interfacial area arises primarily from the small scales. The total area–volume ratio can be expected to be Reynolds-number and Schmidt-number dependent, as well as flow-geometry dependent, in general.

4. Conclusions

Scale-local and cumulative area–volume measures of fluid interfaces enable an examination of the interfacial structure as a function of scale or across a range of scales, respectively. Demonstration of these measures on mixed-fluid interfaces derived from concentration-field measurements has resulted in findings with immediate impact on the study of interfacial self-similarity in turbulence. While the cumulative area–volume behaviour is scale dependent, as evidenced in the area–volume ratio $\Omega_3(\lambda)$ and the dimension $D_3(\lambda)$, the scale-local structure exhibits self-similarity in terms of the area–volume density $g_3(\lambda)$. The latter separates the small-scale properties from the large-scale behaviour. The scale dependence in the cumulative structure arises from the large scales, while the self-similar structure corresponds to the small-scale area–volume contributions.

The present findings on interfacial area–volume properties demonstrate an example of turbulent-flow conditions, above the mixing transition, for which scale dependence in the cumulative structure is consistent with self-similarity in the scale-local structure. This suggests, for example, that in turbulent flows where large-scale effects are present, observations of scale dependence based on $D_3(\lambda)$ alone will need to be examined also in terms of the scale-local area–volume density $g_3(\lambda)$. The present findings show that scale dependence in the cumulative interfacial structure can be consistent with the original ideas of Richardson (1922), when the scale-local interfacial structure exhibits self-similarity. Because the small scales are associated with the largest area–volume density, they are essential to quantify the total area–volume ratio of the interfaces. The observed self-similarity in the scale-local structure at small scales provides the key ingredient to extrapolate the interfacial area–volume behaviour to higher Reynolds numbers.

This work is supported by the National Science Foundation through Career Award Grant CTS-9875036 (Dr C. Chen and Dr J. Foss, Program Managers) and by the Air Force Office of Scientific Research through Grants 01-NA-147 and 01-NA-440 (Dr T. Beutner, Program Manager), and is part of a research program on turbulent flows and fluid interfaces. The authors are grateful to J. Hearn, B. McDonald, K. Sreenivasan, R. Thayne, E. Villermaux and the referees for their comments.

REFERENCES

Brown, G. L. & Roshko, A. 1974 On density effects and large scale structure in turbulent mixing layers. *J. Fluid Mech.* **64**, 775–816.

Catrakis, H. J. 2000 Distribution of scales in turbulence. *Phys. Rev.* E **62**, 564–578.

Catrakis, H. J., Aguirre, R. C., Ruiz-Plancarte, J., Thayne, R. D., McDonald, B. A. & Hearn, J. W. 2002 Large-scale dynamics in turbulent mixing and the three-dimensional space–time behaviour of outer fluid interfaces. *J. Fluid Mech.* To appear.

Catrakis, H. J. & Bond, C. L. 2000 Scale distributions of fluid interfaces in turbulence. *Phys. Fluids* **12**, 2295–2301.

Catrakis, H. J. & Dimotakis, P. E. 1996 Mixing in turbulent jets: scalar measures and isosurface geometry. *J. Fluid Mech.* **317**, 369–406.

Catrakis, H. J. & Dimotakis, P. E. 1998 Shape complexity in turbulence. *Phys. Rev. Lett.* **80**, 968–971.

Dalziel, S. B., Linden, P. F. & Youngs, D. L. 1999 Self-similarity and internal structure of turbulence induced by Rayleigh–Taylor instability. *J. Fluid Mech.* **399**, 1–48.

Dimotakis, P. E. 2000 The mixing transition in turbulent flows. *J. Fluid Mech.* **409**, 69–98.

Dimotakis, P. E., Catrakis, H. J. & Fourguette, D. C. L. 2001 Flow structure and optical beam

propagation in high-Reynolds-number gas-phase shear layers and jets. *J. Fluid Mech.* **433**, 105–134.

Frederiksen, R. D., Dahm, W. J. A. & Dowling, D. R. 1996 Experimental assessment of fractal scale similarity in turbulent flows. Part 1. One-dimensional intersections. *J. Fluid Mech.* **327**, 35–72.

Frederiksen, R. D., Dahm, W. J. A. & Dowling, D. R. 1997 Experimental assessment of fractal scale similarity in turbulent flows. Part 2. Higher-dimensional intersections and non-fractal inclusions. *J. Fluid Mech.* **338**, 89–126.

Frisch, U. 1995 *Turbulence: The Legacy of A. N. Kolmogorov*. Cambridge University Press.

Gad el Hak, M. 2000 *Flow Control: Passive, Active, and Reactive Flow Management*. Cambridge University Press.

Jumper, E. J. & Fitzgerald, E. J. 2001 Recent advances in aerooptics. *Prog. Aerospace Sci.* **37**, 299–339.

Mandelbrot, B. B. 1975 On the geometry of homogeneous turbulence, with stress on the fractal dimension of the isosurfaces of scalars. *J. Fluid Mech.* **72**, 401–416.

Miller, P. L. & Dimotakis, P. E. 1991 Stochastic geometric properties of scalar interfaces in turbulent jets. *Phys. Fluids* A **3**, 168–177.

Paizis, S. T. & Schwarz, W. H. 1974 An investigation of the topography and motion of the turbulent interface. *J. Fluid Mech.* **63**, 315–343.

Pope, S. B. 1988 The evolution of surfaces in turbulence. *Intl J. Engng Sci.* **26**, 445–469.

Prasad, R. R. & Sreenivasan, K. R. 1990 Quantitative three-dimensional imaging and the structure of passive scalar fields in fully turbulent flows. *J. Fluid Mech.* **216**, 1–34.

Richardson, L. F. 1922 *Weather Prediction by Numerical Process*. Cambridge University Press.

Roshko, A. 1991 The mixing transition in free shear flows. In *The Global Geometry of Turbulence* (ed. J. Jiménez), pp. 3–11. Plenum.

Sreenivasan, K. R. 1991 Fractals and multifractals in fluid turbulence. *Annu. Rev. Fluid. Mech.* **23**, 539–600.

Sreenivasan, K. R. & Antonia, R. A. 1997 The phenomenology of small-scale turbulence. *Annu. Rev. Fluid. Mech.* **29**, 435–472.

Sreenivasan, K. R. & Meneveau, C. 1986 The fractal facets of turbulence. *J. Fluid Mech.* **173**, 357–386.

Sreenivasan, K. R., Ramshankar, R. & Meneveau, C. 1989 Mixing, entrainment and fractal dimensions of surfaces in turbulent flows. *Proc. R. Soc. Lond.* A **421**, 79–108.

Takayasu, H. 1982 Differential fractal dimension of random walk and its applications to physical systems. *J. Phys. Soc. Japan* **51**, 3057–3064.

Vassilicos, J. C. & Hunt, J. C. R. 1991 Fractal dimensions and spectra of interfaces with application to turbulence. *Proc. R. Soc. Lond.* A **435**, 505–534.

Villermaux, E. & Innocenti, C. 1999 On the geometry of turbulent mixing. *J. Fluid Mech.* **393**, 123–147.

Welander, P. 1955 Studies on the general development of motion in a two-dimensional, ideal fluid. *Tellus* **7**, 141–156.

Yoda, M., Hesselink, L. & Mungal, M. G. 1994 Instantaneous three-dimensional concentration measurements in the self-similar region of a round high-Schmidt-number jet. *J. Fluid Mech.* **279**, 313–350.